


Waveform Codesign for Radar–Communication Spectral Coexistence via Dynamic Programming

SHAMMI A. DOLY 

ALEX R. CHIRIYATH 

HANS D. MITTELMANN 

DANIEL W. BLISS , Fellow, IEEE
Arizona State University, Tempe, AZ USA

SHANKARACHARY RAGI , Senior Member, IEEE
South Dakota School of Mines and Technology, Rapid City, SD USA

In this article, we develop a new waveform codesign approach for radar–communications spectral coexistence using a decision-theoretic framework called *partially observable Markov decision process* (POMDP). The POMDP framework’s natural look-ahead feature allows us to trade off short-term for long-term performance, which is necessary in waveform codesign problems with competing objectives and dynamic user needs. As POMDPs are computationally intractable, we extend two approximation methods called *nominal belief-state optimization* and *random-sampling multipath hypothesis propagation* to make the codesign approaches tractable.

Manuscript received 1 June 2021; revised 12 October 2021 and 20 January 2022; released for publication 13 March 2022. Date of publication 29 March 2022; date of current version 11 October 2022.

DOI. No. 10.1109/TAES.2022.3162567

Refereeing of this contribution was handled by S. Blunt.

The work of Shammi A. Doly, Shankarachary Ragi, and Hans D. Mittelmann was supported by the Air Force Office of Scientific Research under Grant FA9550-19-1-0070.

Authors’ addresses: Shammi A. Doly, Alex Chiriyath, and Daniel W. Bliss are with the School of Electrical, Computer and Energy Engineering, Arizona State University, Tempe, AZ 85287 USA, E-mail: (sdoly@asu.edu; achiriyath@asu.edu; d.w.bliss@asu.edu); Hans D. Mittelmann is with the School of Mathematical and Statistical Sciences, Arizona State University, Tempe, AZ 85287 USA, E-mail: (mittelmann@asu.edu); Shankarachary Ragi is with the Department of Electrical Engineering, South Dakota School of Mines and Technology, Rapid City, SD 57701 USA, E-mail: (shankarachary.ragi@sdsmt.edu). (*Corresponding author: Shammi A. Doly.*)

This work is licensed under a Creative Commons Attribution 4.0 License. For more information, see <https://creativecommons.org/licenses/by/4.0/>

I. INTRODUCTION

Spectral congestion is forcing legacy radar band users to investigate cooperation and codesign methods with a growing number of communication applications [1]. The codesign of radar and wireless communication systems faces several challenges: interference, radar, communication decoupling, and dynamic user (radar and communications) requirements. In [2] and [3], a detailed overview of the challenges and research directions in the “spectral” coexistence of radar and communications is provided. In [4], the quality of the radar return and the communication rate is mainly determined by the waveform’s spectral shape. Moreover, one of the critical challenges for any waveform design method is to meet dynamic user needs. In this article, we develop waveform shaping methods that are adaptive and can trade off between competing performance objectives to address these challenges. A waveform design method can most effectively meet the dynamic user needs if it predicts the future user needs and allocates the resources accordingly. Previous research has considered waveform design for joint radar–communications systems (see, e.g., [5] and [6]). However, the existing methods often do not meet dynamic performance requirements, as they tend to be *greedy* in that they only maximize short-term performance for immediate benefits. For problems with dynamic performance requirements, long-term performance is critical as decisions (to choose a particular waveform) at the current time epoch may lead to regret in the future. To address these challenges, we develop an adaptive waveform design method for joint radar–communications systems based on the theory of *partially observable Markov decision process* (POMDP) [7], [8]. Specifically, we formulate the waveform design problem as a POMDP [8], after which the design problem becomes a matter of solving an optimization problem. In essence, the POMDP solution provides us with the optimal decisions on the waveform design parameters [9]. The optimization problems resulting from POMDPs are hard to solve precisely; specifically, these problems are PSPACE-complete [10]. The optimization problems resulting from POMDP formulation are typically reformulated as *dynamic programming* problems, which allows us to apply *Bellman’s principle of optimality*, leading to a plethora of approximation methods called *approximate dynamic programming* (ADP) methods, as surveyed in [7]. In this study, we adopt two different ADP approaches called *nominal belief-state optimization* (NBO) [7] and *random-sampling multipath hypothesis propagation* (RS-MHP) [11], [12] to maximize the reward in the long-horizon decision problems. RS-MHP methods are a variant of the existing broad class of Monte Carlo tree search methods. The POMDP framework has a natural look-ahead feature, i.e., it can trade off short-term for long-term performance. This feature lets the POMDP naturally anticipate the dynamic user needs and optimize the resources (waveforms) to actively meet the user’s needs. Typically, one studies these adaptive methods under “cognitive radio (radar),” which has a rich literature. The current waveform design problem is related to a class of

problems called *adaptive sensing*, where the POMDP was already a proven effective framework [9], [13]. However, this article brings formalism to these methods by posing the waveform design problem as a POMDP. Recently, POMDPs were used in [14] to develop adaptive methods for “cognitive radar,” but in a different context, where the focus was on optimizing radar measurement times and not on waveform shaping.

A. Literature Review

Modern spectrum sharing techniques proposed waveform codesign and operation as a necessary construct for joint radar–communications [15], [16]. Various methods employ optimization theory to select a jointly optimal waveform [17]–[19] or jointly maximizing information criteria for radar and orthogonal frequency-division multiplexing (OFDM) communication users to minimize mutual interference for dynamic bandwidth allocation [20]. Other avenues for codesign have also been investigated [21]–[30]. Most modern codesign approaches do not take the long-term needs of the system into consideration. The proposed POMDP-based waveform codesign framework is able to evaluate the needs of the system into the future and trade performance in the short term versus the long term.

Cognitive techniques in radar were primarily used for enhanced dynamic behavior in complex environments [31], [32], but researchers have begun to look at cognitive radar as a solution to the spectral scarcity problem via radar scheduling [33] or employing cognitive radio spectrum sensing techniques, emitter localization, and power allocation to avoid interference [34]–[39]. Others have investigated cognitive radar as a solution to the spectral congestion problem [40]–[43]. Most research efforts tend to adaptively use the spectrum to avoid interference. Such methods are akin to the traditional spectrum sharing solution of isolation in space, time, and/or frequency, which can limit joint system performance as opposed to a codesign approach, where both the systems cooperatively utilize the spectrum. Codesign approaches, such as our POMDP-based approach, show better joint system performance due to better cooperation between systems.

Relationships between radar estimation sidelobe ambiguity and communication channel coding were previously studied [44]. Others have suggested specific coding techniques with favorable properties such as finite Heisenberg–Weyl groups [45], Golay waveforms with Doppler resilient properties [46], and complementary sequences [47]. These approaches tend to prioritize the performance of one system over the other and as such are suboptimal in performance to most modern codesign approaches.

OFDM was investigated as a viable option in vehicle-to-vehicle applications [48]–[51], software-defined radio architectures [52], etc. However, results show conflicting cyclic prefix requirements, data-dependent ambiguities, and trouble-mitigating peak-to-average power ratio (PAPR) for typical radar power requirements. Researchers focused on developing joint systems that could mitigate the effects

of these problems, such as suppressing sidelobes [53], maintaining a constant envelope [54], or reducing PAPR [55]. An OFDM approach is fundamentally more favorable to communication system performance, and most research efforts lie in improving radar performance to an acceptable level. However, codesign approaches such as ours are more beneficial in the long term due to them giving both systems equal importance.

B. Key Contributions

The key contributions of this study are as follows:

- 1) We formulate the joint radar waveform codesign problem as a POMDP.
- 2) We extend ADP methods NBO and RS-MHP to solve the waveform design problem posed as the POMDP.
- 3) We implement the POMDP-based waveform codesign algorithms in simulated environments and conduct a numerical study to quantify the impact of the planning horizon on the performance of our methods.

A preliminary version of the parts of this article was published as [8]. This article differs from the conference article [8] in the following ways: 1) along with the previous numerical results in [8], we conduct an empirical study to assess the impact of the planning horizon H in the POMDP on the radar and communication performance and 2) we extend a new ADP approach RS-MHP [11], [12] to solve the waveform codesign problem and benchmark its performance against the NBO approach we previously used in [8].

II. JOINT RADAR–COMMUNICATION PREMISE

A. Successive Interference Cancellation Receiver Model

Table I shows the notations employed in this article. In this article, we use an optimal multiuser receiver model called successive interference cancellation (SIC) [2], [57] to remove the communication signal from the radar return. Based on the prior observations of the radar target range (or time delay) up to some random fluctuation (also called process noise) $n_{\text{proc}}(t)$ as a zero-mean random variable, we generate the radar return. Then, we subtract the predicted radar return from the joint radar–communication signal received. After suppressing the radar return, the receiver then decodes and removes the communication signal from the received signals. It is this receiver model that causes communication performance to be closely tied to the radar waveform spectral shape. The block diagram of the joint radar–communication system considered in this scenario is shown in Fig. 1. When applying SIC, the interference residual plus noise signal $n_{\text{int+n}}(t)$, from the communications receiver’s perspective, is given by [3], [58]

$$\begin{aligned} n_{\text{int+n}}(t) &= n(t) + n_{\text{resi}}(t) \\ &= n(t) + \sqrt{\|a\|^2 P_{\text{rad}}} n_{\text{proc}}(t) \frac{\partial x(t - \tau)}{\partial t} \end{aligned} \quad (1)$$

TABLE I
Survey of Notation

Variable	Description
B	Total system bandwidth
B_{rms}	Root-mean-squared radar bandwidth
B_{com}	Communications-only subband
P_{rad}	Radar power
T_{temp}	Effective temperature
b	Communications propagation loss
P_{com}	Communications power
P_{rad}	Communications power
$x(t)$	Unit-variance transmitted radar signal
a	Combined antenna gain
N	Number of samples
σ_{CRLB}^2	Cramer-Rao lower bound
σ_{noise}^2	Thermal noise
σ_{proc}^2	Process noise variance
TB	Time-bandwidth product
δ	Radar duty factor
w	Measurement noise
ζ_k	Mean vector noise
τ	Time delay to m^{th} target
α	Weighting parameter
R_{comm}	Communications rate
R_{est}	Radar estimation rate
P_k	Error covariance matrix
T_{pri}	Pulse repetition interval
H	Planning horizon length

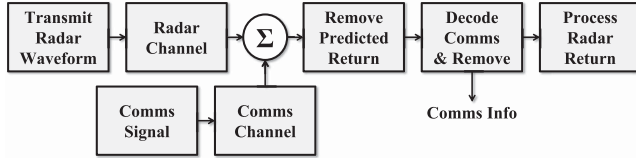


Fig. 1. Joint radar–communication system block diagram for the SIC scenario. The radar and communication signals have two effective channels, but arrive converged at the joint receiver. The radar signal is predicted and removed, allowing a reduced rate communication user to operate. Assuming near-perfect decoding of the communication user, the ideal signal can be reconstructed and subtracted from the original waveform, allowing for unimpeded radar access.

and

$$\|n_{int+n}(t)\|^2 = \sigma_{noise}^2 + a^2 P_{rad} (2\pi B_{rms})^2 \sigma_{proc}^2 \quad (2)$$

where $n_{proc}(t)$ is the process noise with variance σ_{proc}^2 .

B. Radar Estimation Rate

To measure spectral efficiency for radar performance, we developed a new metric recently called *radar estimation rate*, which is formally defined as the minimum average data rate required to provide the time-dependent estimates of system or target parameters, for example, target range [3], [58], [59]. The radar estimation rate is expressed as

follows:

$$R_{est} = I(\mathbf{x}; \mathbf{y})/T_{pri} \quad (3)$$

where $I(\mathbf{x}; \mathbf{y})$ is the mutual information between random vectors \mathbf{x} and \mathbf{y} and $T_{pri} = T_{pulse}/\delta$ is the pulse repetition interval of the radar system; T_{pulse} is the radar pulse duration and δ is the radar duty factor. This rate allows the construction of joint radar–communication performance bounds and allows future system designers to score and optimize systems relative to a joint information metric. For a simple range estimation problem with a Gaussian tracking prior, this takes the form [2], [3], [60]

$$R_{est} = (1/2T) \log_2(1 + \sigma_{proc}^2/\sigma_{CRLB}^2) \quad (4)$$

where σ_{proc}^2 is the range-state process noise variance and σ_{CRLB}^2 is the Cramér–Rao lower bound (CRLB) for range estimation given by [3], [58], [59]

$$\sigma_{CRLB}^2 = \frac{\sigma_{noise}^2}{8\pi^2 B_{rms}^2 T_p B P_{rad,rx}} \quad (5)$$

where σ_{noise}^2 is the noise variance or power, T_p is the radar pulse duration, B_{rms} is the radar waveform root-mean-square (RMS) bandwidth, and $P_{rad,rx}$ is the radar receive power, which is inversely proportional to the distance of the target from the joint node. Immediately apparent is the similarity of the above equation to Shannon’s channel capacity, eq. [3], [58], [59], where the ratio of the source uncertainty variance to the range estimation noise variance forms a pseudo-signal-to-noise ratio (SNR) term. In (4), the estimation rate is inversely proportional to the distance of the target from the joint node. As discussed later, we design the waveform parameters over the planning horizon while accounting for the varying estimation rate due to target’s motion.

C. Inner Rate Bounds

We measure the performance of the system with two metrics: communication information rate bound and radar estimation rate bound (discussed in the previous section). The joint radar–communication performance bounds developed in [3], [58], and [59] considered only local radar estimation error, therefore making simplified assumptions about the radar waveform. In [4], the results were generalized to include the formulation of an optimal radar waveform for both the global radar estimation rate performance and the consideration of in-band communication users forced to mitigate radar returns. After the SIC process, some radar residual will be left in the communication signal (due to error in the predicted target location and the actual target location). If $R_{est} \approx 0$ is sufficiently low, then the communication operates according to the bound determined by the isolated communication system [2]. The highest possible communication rate when decoding the post-SIC received signal is given by

$$\tilde{R}_{com} \leq B \log_2 \left[1 + \frac{b^2 P_{com}}{\sigma_{noise}^2} \right]. \quad (6)$$

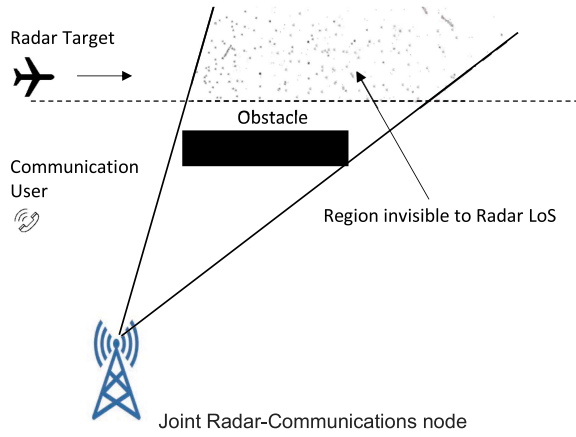


Fig. 2. Target tracking problem scenario.

If \tilde{R}_{com} is sufficiently low for a given transmit power, then the communication signal can be decoded and subtracted completely from the underlying signal, so that the radar parameters can be estimated without contamination

$$\tilde{R}_{\text{com}} \leq B \log_2 \left[1 + \frac{b^2 P_{\text{com}}}{\sigma_{\text{noise}}^2 + a^2 P_{\text{rad}} (2\pi B_{\text{rms}})^2 \sigma_{\text{proc}}^2} \right]. \quad (7)$$

In this regime, the corresponding estimation rate bound R_{est} is given by (4). An achievable rate lies within the imaginary triangle constructed by (4), (6), and (7).

III. PROBLEM SPECIFICATION

We consider a case study with a radar target, communication user, and the joint node, as shown in Fig. 2. We consider a single clutter condition, as shown in Fig. 2, where an obstacle may occlude the line of sight (LOS) of the target from the joint node. Total clutter residue acts as extra additive noise in the system, which causes the channel to appear more degraded. Radar estimation rates are also reduced (radar and communication overlap) once the clutter occludes the target. We do not consider any external interference or a jamming condition in this article. We will develop our POMDP framework for this case study, which can be easily generalized and extended to other problem scenarios. This particular case study allows us to show the qualitative and quantitative benefits of the POMDP in adaptive waveform design. The key components in the waveform design algorithm based on the POMDP are shown in Fig. 3. The POMDP planner evaluates the belief-state (posterior distribution over the state space updated according to Bayes' rule) of the system, uses an ADP method to solve the POMDP approximately, and produces optimal or near-optimal decisions on waveform parameters; details are discussed later. Our objective is to design the shape of the waveforms over time to maximize the system's performance. First, we begin with a unimodular chirp waveform $\exp[j(\pi B/T)(t^2)]$. We control the spectral shape of this chirp signal to maximize joint performance. We first sample the chirp signal and collect m samples in the frequency domain to achieve this. Let $X = (X(f_1), \dots, X(f_m))^T$ be

the discretized signal in the frequency domain at frequencies f_1, \dots, f_m . Let $u = (u(1), \dots, u(m))^T$ be an array of spectral weights we will optimize as discussed below, where $u(i) \in [0, 1] \forall i$. We control the chirp signal's spectral shape by multiplying (i.e., dot product) the signal with the spectral weights in the frequency domain, i.e., the resulting signal is given by $X(f_i)u(i) \forall i$.

IV. POMDP FORMULATION FOR JOINT WAVEFORM CODESIGN

To pose any decision-making problem as a POMDP, we need to define the POMDP ingredients, namely, states, actions, state-transition law, observations and observation law, and reward function, in the context of the particular problem at hand. The following is a description of the POMDP ingredients as defined specific to our waveform design problem. Hereafter, we model the system dynamics as a discrete-event process, where k represents the discrete-time index.

States: State at time k is defined as $x_k = (\chi_k, \xi_k, P_k)$, where χ_k represents the target state, which includes the location, velocity, and the acceleration of the target, and (ξ_k, P_k) represents the state of the tracking algorithm, e.g., Kalman filter, where ξ_k is the mean vector and P_k is the covariance matrix.

Actions: Actions are the waveform spectral weights vector u_k , at time k , as defined previously.

State-transition law: χ_k evolves according to a target motion model *near-constant velocity model* [9] captured by $\chi_{k+1} = F \chi_k + n_k$, where F is a transition matrix, and $n_k = n_{\text{proc}}(t = k)$ is the process noise described in Section II-A, which is modeled as a Gaussian process. ξ_k and P_k evolve according to Kalman filter equations.

Observation law: $z_k^{\text{Targ}} = G \chi_k + w_k$ (if not occluded) and $z_k^{\text{Targ}} = w_k$ (if occluded), where G is a transition matrix and w_k is the measurement noise, modeled as a Gaussian process. Specifically, $w_k \sim \mathcal{N}(0, R_k)$, where R_k is the noise covariance matrix, where the entries in the matrix scale (increase) with the distance between the joint node (or sensor node) and the target. We assume the other state variables to be fully known.

Reward function: The reward function rewards the decision u_k taken at time k given the state of the system is x_k , as defined in the following:

$$R(x_k, u_k) = \alpha R_{\text{est}}(x_k, u_k) + (1 - \alpha) R_{\text{comm}}(x_k, u_k) \quad (8)$$

where R_{est} is the radar estimation rate [4], R_{comm} is the communication data rate, and $\alpha \in [0, 1]$ is a weighting parameter. The dependence of the rates on the waveform spectral weights u_k is explained as follows. Both the rates $R_{\text{est}}(x_k, u_k)$ and $R_{\text{comm}}(x_k, u_k)$ are a function of the RMS bandwidth B_{rms} of the waveform, as can be seen from (4), (5), and (7). The RMS bandwidth clearly depends on the shape of the waveform spectrum, which is determined by the waveform spectral weights u_k .

Belief state: We maintain and update the posterior distribution over the state space (as the actual state is not fully

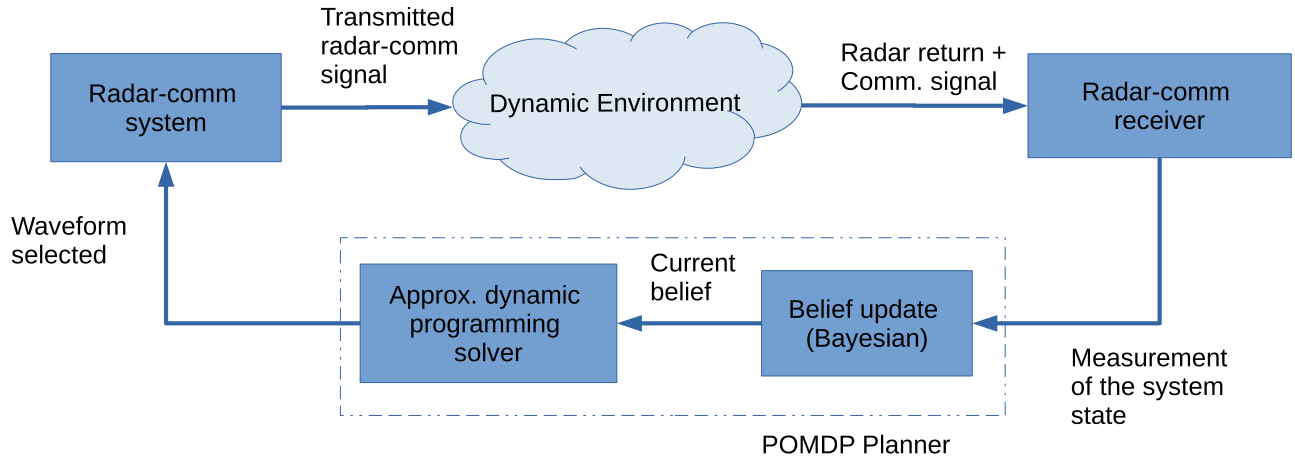


Fig. 3. Adaptive waveform optimization in a dynamic environment.

observable), also known as the “belief state” given by $b_k = (b_k^x, b_k^\xi, b_k^p)$, where $b_k^\xi(x) = \delta(x - \xi_k)$, $b_k^p(x) = \delta(x - P_k)$, and $b_k^x = \mathcal{N}(\xi_k, P_k)$. Here, we know the state of the tracking algorithm, so belief states corresponding to these states are just delta functions, whereas the target state is modeled as a Gaussian distribution with ξ_k and P_k as the mean vector and the error covariance matrix, respectively. Our goal is to optimize the actions over a long time horizon (of length H) to maximize the expected cumulative reward. The objective function (to be maximized) is given by $J_H = \mathbb{E}[\sum_{k=0}^{H-1} R(x_k, u_k)]$. However, we can also write J_H in terms of the belief states as

$$J_H = \mathbb{E} \left[\sum_{k=0}^{H-1} r(b_k, u_k) \mid b_0 \right] \quad (9)$$

where $r(b_k, u_k) = \int R(x, u_k) b_k(x) dx$ and b_0 is the initial belief state. Let $J_H^*(b)$ represent the optimal objective function value, given the initial belief state b . Therefore, the optimal action policy at time k is given by $\pi^*(b_k) = \arg \max_u Q(b_k, u)$, where $Q(b_k, u) = r(b_k, u) + \mathbb{E}[J_H^*(b_{k+1}) \mid b_k, u]$, which is also called the Q -value. A detailed description of the POMDP and its solution can be found in [7] and [9]. POMDP formulations are notorious for their high computational complexity (PSPACE-complete [10]), particularly because it is near impossible to obtain the above-discussed Q -value in real time [9]. Most ADP methods approximate the Q -value [7]. We adopt two ADP approaches: NBO [9] and RS-MHP [11], [12].

A. POMDP Solution via NBO

With NBO approximation, the POMDP formulation leads to the following optimization problem:

$$\max_{u_k, k=0, \dots, H-1} \sum_{k=0}^{H-1} r(\tilde{b}_k, u_k) \quad (10)$$

where $\tilde{b}_k, k = 0, \dots, H-1$, is a sequence of readily available “nominal” belief states, as opposed to b_k s which are random variables, obtained from the NBO approach. In

Algorithm 1: NBO Algorithm.

Require Find the (sub)optimal spectral weights using the NBO approach at a discrete-time index k

- 1: Initialize the environment, noise intensities, process noise matrix
 - 2: $H \leftarrow$ length of planning horizon
 - 3: $k \leftarrow$ discrete-time index
 - 4: Initialize action vector u_k to random spectral weights, and the prior belief state is b_k
 - 5: Define the NBO objective/reward function: $J_{NBO}(u_k) \leftarrow$ cumulative (over planning horizon H) weighted average of the estimation and communications rates [see (10)], where the estimation and communications rates are evaluated assuming the future target belief states are evaluated with all noise variables collapsing to their “nominal values”
 - 6: **for each** k **do**
 - 7: Update the target belief state b_k (posterior distribution) via Kalman–Bayes equations using the target state measurements received at k
 - 8: Solve the below NBO optimization problem to obtain the (sub)optimal weights using MATLAB’s *fmincon*: $u_k^* \leftarrow \arg \max_u J_{NBO}(u)$
 - 9: Design the spectral shape of the chirp signal using optimal weights u_k^* , as discussed in Section III
 - 10: **end for** $\triangleright k$
-

NBO, the expectation is replaced by a sample state trajectory generated with an assumption that the future noise variables in the system collapse to the nominal or mean values (see Fig. 4), thus making the above objective function deterministic. The NBO method was developed to solve a unmanned aerial vehicle path optimization problem, which was posed as a POMDP [9]. The POMDP generalizes the long-horizon optimal control problem described in [11] in that the system state is assumed to be “partially” observable,

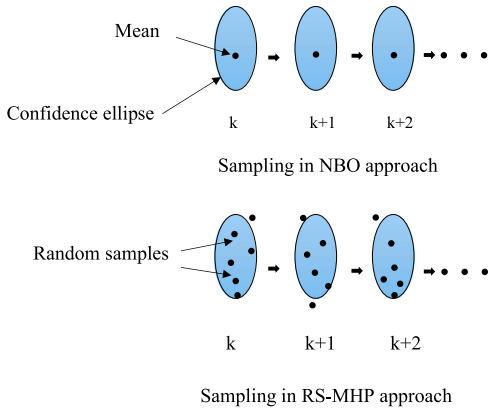


Fig. 4. Sampling in NBO versus RS-MHP approach.

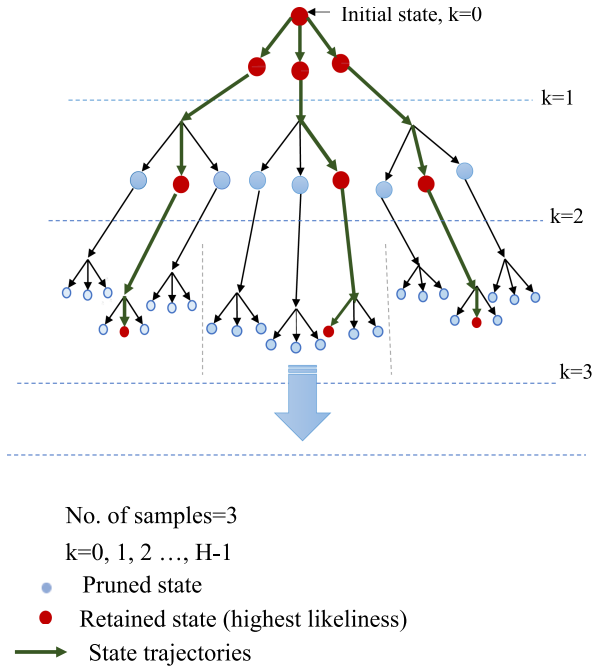


Fig. 5. Sampling in the RS-MHP approach with pruning (three nodes allowed to remain at each stage).

which is inferred via the use of noisy observations and Bayes rules. Although the performance of the NBO approach was satisfactory in that it allowed to obtain reasonably optimal reward commands for the decision problem to be received, it ignored the uncertainty due to noise disturbances, thus leading to an inaccurate evaluation of the objective function. This challenge can be overcome by the RS-MHP approach, as discussed in the following.

B. POMDP Solution via RS-MHP

The tree-like sampling of the states in the RS-MHP approach, as shown in Figs. 4 and 5, allows us to incorporate the uncertainty of the state evolution into the decision-making criteria, albeit with the increased computational burden compared to NBO. However, the sampling approach allows us to trade off between the computational intensity and the solution's optimality (determined by our choice

Algorithm 2: RS-MHP Algorithm.

Require Find the (sub)optimal spectral weights using the RS-MHP approach at a discrete-time index k

- 1: Initialize the environment, noise intensities, process and measurement matrix
 - 2: $H \leftarrow$ length of planning horizon
 - 3: $k \leftarrow$ discrete-time index
 - 4: $N \leftarrow$ sampling size (as described in Section IV-B)
 - 5: $M \leftarrow$ retained states after pruning [as described in (11)]
 - 6: Initialize action vector u_k to random spectral weights, and the prior belief state be b_k
 - 7: Define the RS-MHP objective/reward function: $J_{\text{RS-MHP}}(u_k) \leftarrow$ cumulative (over planning horizon H) reward function averaged over all the possible state trajectories or tree branches [see (11)], where the estimation and communication rates are evaluated assuming that the future target belief states are evaluated using the sampling procedure discussed in Section IV-B.
 - 8: **for each** k **do**
 - 9: update the target belief state b_k (posterior distribution) via Kalman-Bayes equations using the target state measurements received at time k
 - 10: Solve the below optimization problem to obtain the (sub)optimal weights using MATLAB's $fmincon: u_k^* \leftarrow \arg \max_u J_{\text{RS-MHP}}(u)$
 - 11: Design the spectral shape of the chirp signal using optimal weights u_k^* , as discussed in Section III.
 - 12: **end for** $\triangleright k$
-

of the number of samples/branches in RS-MHP). In the RS-MHP approach, we sample the probability distribution of the state of the system (a random variable) N times at each time step and generate a sampling tree, as shown in Fig. 5 (here, $N = 3$). To avoid the exponential growth of the state sample nodes in this approach, at each time step, we retain only M sample states and prune the remaining samples. If the number of sample states at a given time instance is less than or equal to M , we do not perform pruning. Fig. 5 shows an illustration of the above branch pruning strategy for a scenario with $N = 3$ and $M = 3$. We prune the tree branches based on their likelihood indices [11], [12], i.e., we retain the top M branches at each time step with the highest sample probabilities.

We approximate the expectation with an average over the possible state trajectories or tree branches as follows:

$$J_{\text{RS-MHP}} = \frac{1}{M} \sum_{i=1}^M \left(\mathbb{E} \left[\sum_{k=0}^{H-1} r(x_k^i, u_k) \mid b_0 \right] \right) \quad (11)$$

where x_k^i represents the sample state node from the i th trajectory at time k . Clearly, as $N \rightarrow \infty$ and $M \rightarrow \infty$,

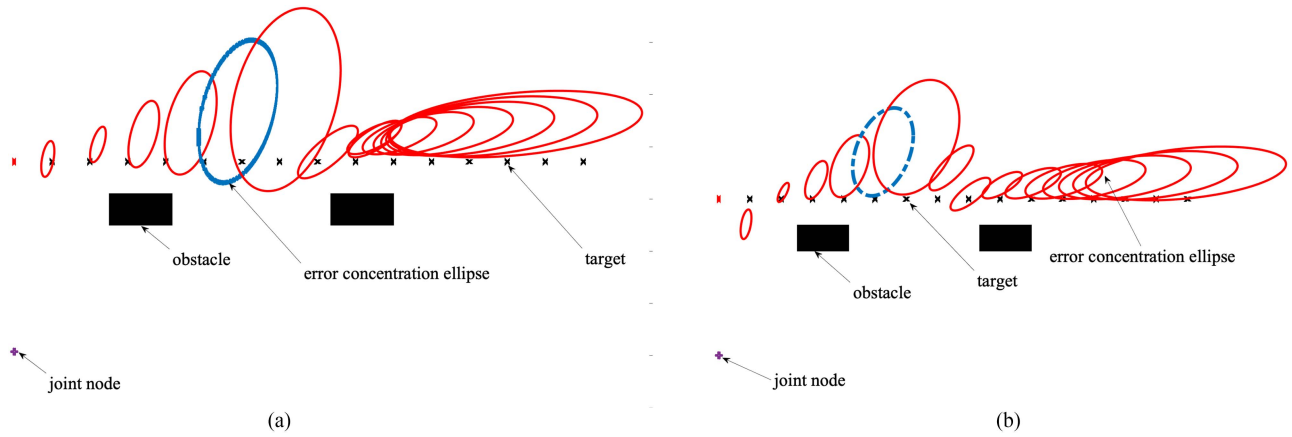


Fig. 6. Error concentration ellipse (95% confidence) of the dynamic target at different locations in both myopic ($H = 1$) and nonmyopic ($H > 1$) approaches for $\alpha = 0.5$ by red lines. The number of iteration indexes is considered $k = 15$ to demonstrate which locations match which ellipses more precisely. For example, the solid blue line shows the error concentration ellipse at the time index $k = 5$ for $H = 1$, and the error concentration ellipse for $H = 9$ at the time index $k = 5$ is shown by the blue-dotted line. We see that with the nonmyopic method ($H > 1$), we could minimize the size of the error concentration ellipse as the target tracking error as determined by the spectral mask we chose. (a) Planning horizon $H = 1$. (b) Planning horizon $H = 9$.

the above approximation converges to the true objective function in (9).

V. SIMULATION AND RESULTS

We study the efficacy of the aforementioned waveform codesign methods in a scenario with two obstacles blocking the LOS between the joint node and the radar target as the target moves from the left to the right, as shown in Fig. 6. Furthermore, we implement the receding horizon control approach while optimizing the decision variables over the moving planning horizon [9]. We implement the NBO and RS-MHP approaches to solve the joint radar waveform optimization problem, in the above context, in MATLAB. We use MATLAB's *fmincon* [61] (an optimization tool in MATLAB) to solve the optimization problems discussed in the previous section. The following are the main objectives of this numerical study.

- 1) Study the optimal radar waveform properties.
- 2) Study the impact of the planning horizon H on the joint performance with respect to the estimation and the communications rates.
- 3) Performance comparison of NBO versus RS-MHP ADP approaches in the nonmyopic approach ($H > 1$).

A. Optimal Radar Waveform Properties

We assume that the joint radar–communication receiver shares a single antenna front end and that the communication signal is received through an antenna sidelobe, while the radar return is received through the same antenna mainlobe, so that the radar and communication receiver gains are not identical. From the simulation results, the SNR in the NBO approach is 19.1419 dB and in the RS-MHP approach is 22.4310 dB. The parameters used in our simulation studies are shown in Table II. In

TABLE II
Parameters for Waveform Design Methods

Parameter	Value
Bandwidth (B)	5 MHz
Center frequency	3 GHz
Effective temperature (T_{temp})	1000 K
Communications range	10 km
Communications power (P_{com})	1 W
Communications receiver Side-lobe gain	20 dBi
Radar antenna gain	30 dBi
Target cross section	10 m ²
Target process standard deviation (σ_{proc})	100 m
Time-bandwidth product (TB)	128
Radar duty factor (δ)	0.01

Fig. 7(a), we show the radar waveform spectral autocorrelation function of the optimized waveform with blending parameter $\alpha = 0.5$ and planning horizon $H = 1$ at a time step $k = 1$. We plot the spectrum of the optimized waveform with $\alpha = 0.5$ along with the original unmasked chirp waveform, as shown in Fig. 7(b). This waveform spectrum shows the joint radar–communication optimal and has more energy at the bandwidth center than the sidebands. The radar waveform spectrum with $\alpha = 0.1$ and $\alpha = 1$ along with the original unmasked chirp waveform is shown in Fig. 8.

B. Effect of Planning Horizon Length on the Joint Performance

We implement the NBO approach for $H = 1$ and $H = 9$, as shown in Fig. 6. In both cases, the size of the error confidence ellipse of the target increases when the target is occluded by the obstacles. The growth of the ellipse size visibly reduces for $H = 9$ compared to $H = 1$. Therefore,

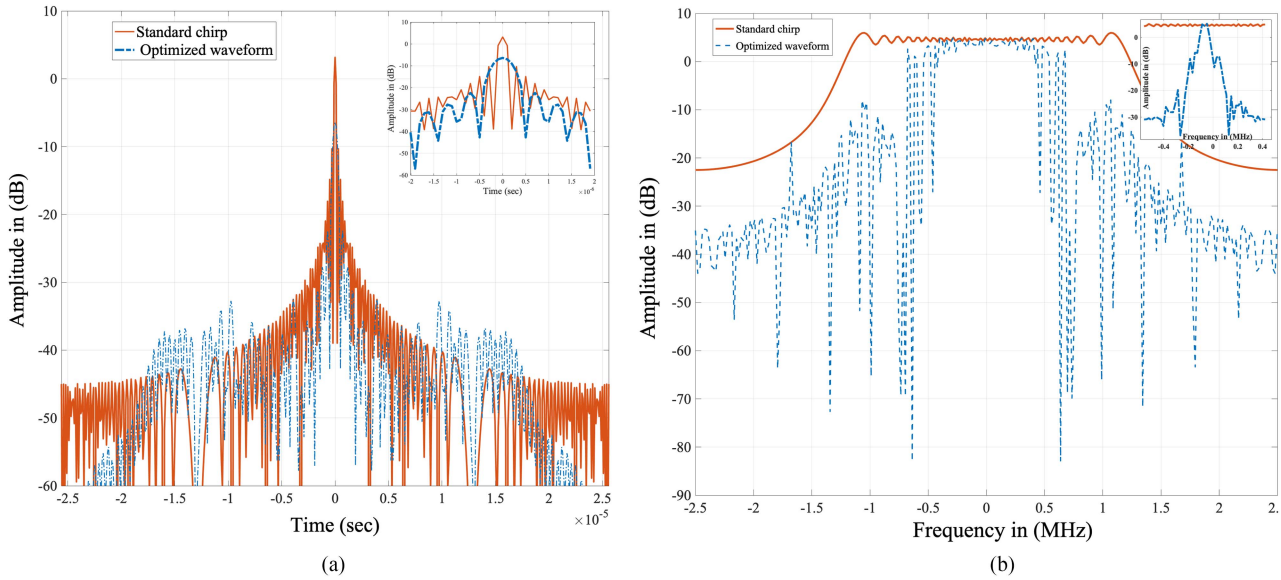


Fig. 7. Optimized waveform versus the standard chirp. (a) Radar waveform autocorrelation function of the optimized waveform with $\alpha = 0.5$ and $H = 1$. (b) Radar waveform spectrum with $\alpha = 0.5$ and $H = 1$. The standard chirp is depicted by the red line, and the optimal waveform spectrum is shown by the blue-dotted line.

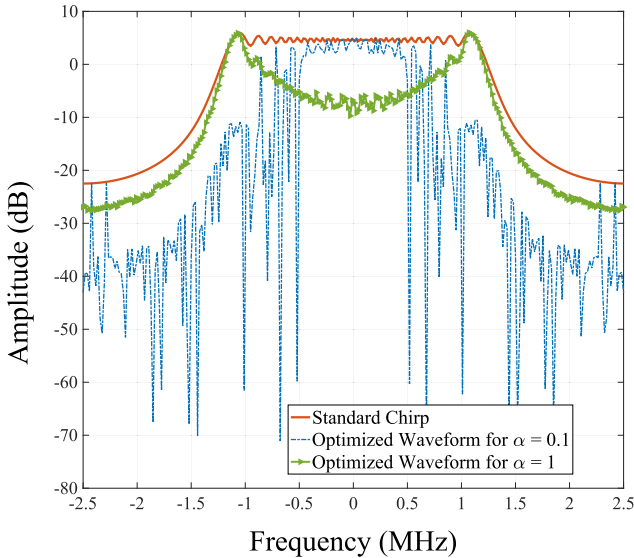


Fig. 8. Original unmasked chirp is depicted by the solid red line. The optimized waveform is depicted for $\alpha = 0.1$ by the blue-dotted line. This waveform spectrum is communication optimal and has more energy in the center of the bandwidth. The optimized waveform is depicted by the green-dashed line for $\alpha = 1$, and this waveform spectrum is radar optimal and has more energy in the edges of the bandwidth.

the nonmyopic method ($H > 1$) has a better capability in keeping the growth of the target-state uncertainty small compared to a myopic approach ($H = 1$). Fig. 9 shows the estimation and the communication rates as a function of the blending parameter α . As expected, α allows us to smoothly trade off between the two rates. Furthermore, in Fig. 10, we plot the estimation rate as a function of time for the above two scenarios with $H = 1$ and $H = 9$, which shows the quantitative benefit of a nonmyopic approach ($H > 1$) over a myopic approach ($H = 1$) in terms of the radar estimation rate. Fig. 11 shows a gradual increase in the

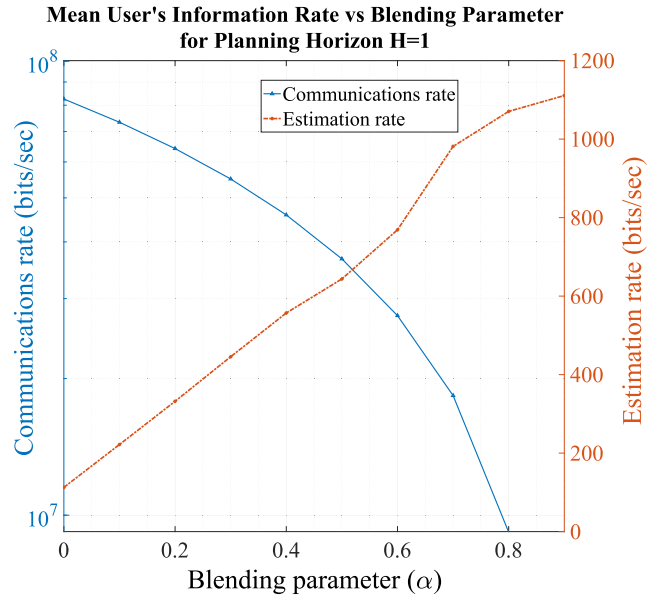


Fig. 9. Rate-rate curve depicting communication and estimation rate versus α . Communication and estimation rate pairs are shown $\alpha \in [0, 1]$.

joint radar-communication performance with increasing H as expected in a nonmyopic approach; however, the computational complexity in solving (9) grows exponentially with H .

C. Performance Comparison of NBO Versus RS-MHP ADP Approaches

Here, we implement the RS-MHP approach for waveform codesign in the same simulation scenario described earlier. Fig. 12 shows the cumulative distribution of the radar estimation rates using RS-MHP and NBO methods for $H = 3$. The figure clearly demonstrates that the RS-MHP approach outperforms the NBO approach and that

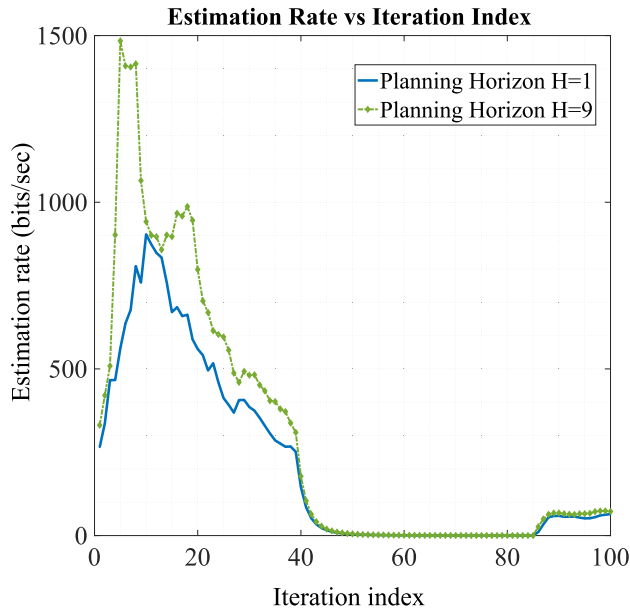


Fig. 10. Estimation rate versus iteration index for both myopic and nonmyopic approaches.

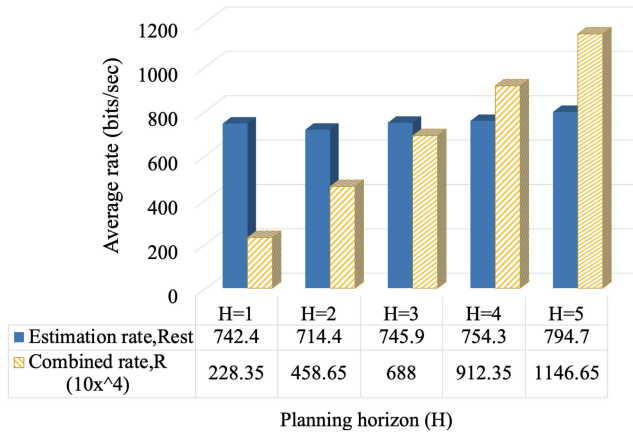


Fig. 11. Average estimation and communication rates versus planning horizon $H \in \{1, 2, 3, 4, 5\}$.

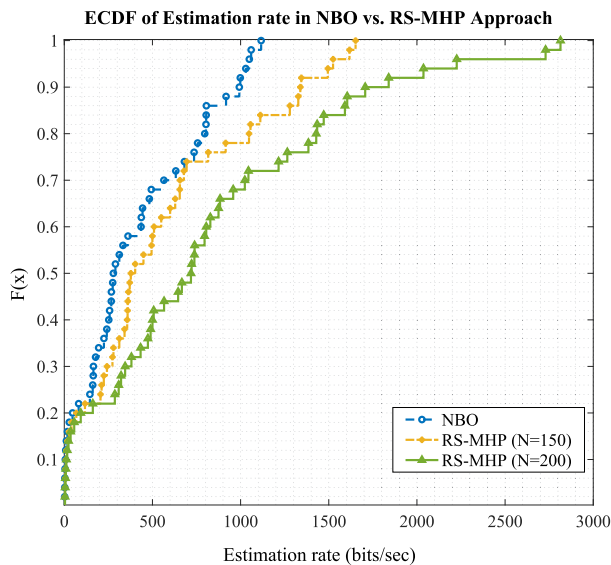


Fig. 12. Cumulative distribution of estimation rate for NBO versus RS-MHP approaches. Here, N represents the number of samples.

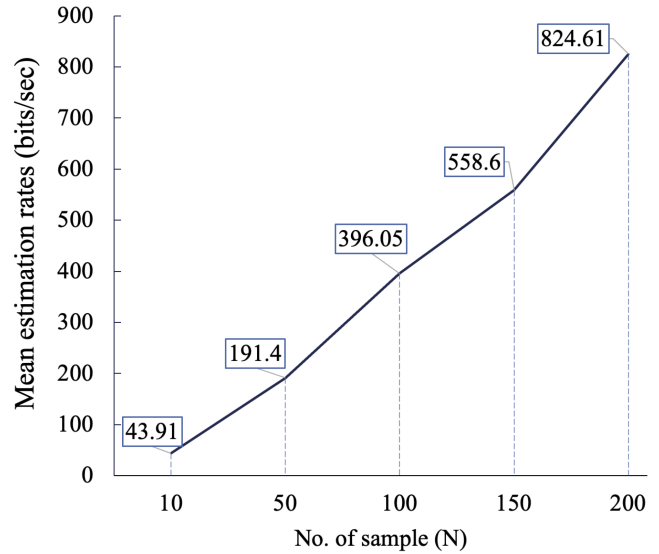


Fig. 13. Mean estimation rate versus number of samples $N \in \{10, 50, 100, 150, 200\}$.

the performance improves as we increase the number of samples N in the RS-MHP approach. Fig. 13 shows the average radar estimation rates for N set to 10, 50, 100, 150, and 200 for $H = 3$. The figure shows a gradual increase in the algorithm's performance (in terms of the estimation rate) with increasing N as expected. This result also suggests that the pruning step in the RS-MHP method would degrade the performance but can provide gains in terms of computational intensity. In summary, our numerical study confirms that the RS-MHP's performance has a clear statistical edge over that of the NBO approach in terms of the estimation rate.

VI. CONCLUSION

In this article, we developed a waveform codesign approach for joint radar–communication systems using a decision-theoretic framework called POMDPs. The goal is to optimize the spectral shape of the radar waveform over time to maximize the joint performance of radar and communications in spectral coexistence measured in terms of radar estimation and communication rates. As most decision-theoretic formulations suffer from the *curse of dimensionality*, we extended two approximation strategies or ADP methods to solve the POMDP: NBO and RS-MHP. Our numerical study confirmed that the POMDP-based nonmyopic waveform codesign approach has a better capability in keeping the growth of target state uncertainty small compared to a myopic approach. We also presented the quantitative benefits, in terms of the communications and the radar estimation rates, of our POMDP-based nonmyopic approach against the traditional myopic approaches. Our results also confirmed a gradual increase in the joint radar–communication performance with increasing planning horizon length, which was expected in a nonmyopic approach. Our numerical studies also confirmed that the ADP approach RS-MHP outperformed the NBO approach in terms of the target estimation rate.

REFERENCES

- [1] J. B. Evans
Shared spectrum access for radar and communications (SS-PARC)
Defense Adv. Res. Projects Agency, Press Release, 2015. [Online]. Available: <http://www.darpa.mil/program/shared-spectrum-access-for-radar-and-communications>
- [2] D. W. Bliss and S. Govindasamy
Adaptive Wireless Communications: MIMO Channels and Networks. Cambridge, U.K.: Cambridge Univ. Press, 2013.
- [3] D. W. Bliss
Cooperative radar and communications signaling: The estimation and information theory odd couple
In *Proc. IEEE Radar Conf.*, May 2014, pp. 50–55.
- [4] B. Paul, A. R. Chiriyath, and D. W. Bliss
Joint communications and radar performance bounds under continuous waveform optimization: The waveform awakens
In *Proc. IEEE Radar Conf.*, May 2016, pp. 865–870.
- [5] P. Chavali and A. Nehorai
Cognitive radar for target tracking in multipath scenarios
In *Proc. Int. Waveform Diversity Des. Conf.*, 2010, pp. 110–114.
- [6] O. Ma, A. R. Chiriyath, A. Herschfeld, and D. Bliss
Cooperative radar and communications coexistence using reinforcement learning
In *Proc. 52nd Asilomar Conf. Signals, Syst. Comput.*, 2018, pp. 947–951.
- [7] E. K. P. Chong, C. Kreucher, and A. O. Hero
Partially observable Markov decision process approximations for adaptive sensing
Discrete Event Dyn. Syst., vol. 19, pp. 377–422, 2009.
- [8] S. A. Doly, A. Chiriyath, H. D. Mittelmann, D. W. Bliss, and S. Ragi
A decision theoretic approach for waveform design in joint radar communications applications
In *Proc. 54th Asilomar Conf. Signals, Syst. Comput.*, Pacific Grove, CA, USA, Nov. 1–4, 2020, pp. 6–11.
- [9] S. Ragi and E. K. P. Chong
UAV path planning in a dynamic environment via partially observable Markov decision process
IEEE Trans. Aerosp. Electron. Syst., vol. 49, no. 4, pp. 2397–2412, Oct. 2013.
- [10] C. H. Papadimitriou and J. N. Tsitsiklis
The complexity of Markov decision processes
Math. Oper. Res., vol. 12, no. 3, pp. 441–450, 1987.
- [11] S. Ragi and H. D. Mittelmann
Random-sampling multipath hypothesis propagation for cost approximation in long-horizon optimal control
In *Proc. IEEE Conf. Control Technol. Appl.*, Montreal, QC, Canada, Aug. 24–26, 2020, pp. 14–18.
- [12] S. Ragi and H. D. Mittelmann
Random-sampling Monte-Carlo tree search methods for cost approximation in long-horizon optimal control
IEEE Control Syst. Lett., vol. 5, no. 5, pp. 1759–1764, Nov. 2021, doi: [10.1109/LCSYS.2020.3043991](https://doi.org/10.1109/LCSYS.2020.3043991).
- [13] S. Ragi, E. K. P. Chong, and H. D. Mittelmann
Mixed-integer nonlinear programming formulation of a UAV path optimization problem
In *Proc. Amer. Control Conf.*, Seattle, WA, USA, 2017, pp. 406–411.
- [14] A. Charlish and F. Hoffmann
Anticipation in cognitive radar using stochastic control
In *Proc. IEEE Radar Conf.*, Arlington, VA, USA, 2016, pp. 1692–1697.
- [15] B. Paul, A. R. Chiriyath, and D. W. Bliss
Survey of RF communications and sensing convergence research
IEEE Access, vol. 5, pp. 252–270, 2017.
- [16] J. R. Guerci, R. M. Guerci, A. Lackpour, and D. Moskowitz
Joint design and operation of shared spectrum access for radar and communications
In *Proc. IEEE Radar Conf.*, May 2015, pp. 761–766.
- [17] X. Wang, A. Hassaniien, and M. G. Amin
Dual-function MIMO radar communications system design via sparse array optimization
IEEE Trans. Aerosp. Electron. Syst., vol. 55, no. 3, pp. 1213–1226, Jun. 2019.
- [18] S. Zhou, X. Liang, Y. Yu, and H. Liu
Joint radar-communications co-use waveform design using optimized phase perturbation
IEEE Trans. Aerosp. Electron. Syst., vol. 55, no. 3, pp. 1227–1240, Jun. 2019.
- [19] F. Wang, H. Li, and M. A. Govoni
Power allocation and co-design of multicarrier communication and radar systems for spectral coexistence
IEEE Trans. Signal Process., vol. 67, no. 14, pp. 3818–3831, Jul. 2019.
- [20] A. Turlapaty and Y. Jin
A joint design of transmit waveforms for radar and communications systems in coexistence
In *Proc. IEEE Radar Conf.*, May 2014, pp. 315–319.
- [21] M. Zatman and M. Scharrenbroich
Joint radar-communications resource management
In *Proc. IEEE Radar Conf.*, May 2016, pp. 1–6.
- [22] Y. L. Sit, C. Sturm, and T. Zwick
One-stage selective interference cancellation for the OFDM joint radar-communication system
In *Proc. 7th German Microw. Conf.*, Mar. 2012, pp. 1–4.
- [23] G. C. Tavik *et al.*
The advanced multifunction RF concept
IEEE Trans. Microw. Theory Techn., vol. 53, no. 3, pp. 1009–1020, Mar. 2005.
- [24] L. Wang, J. McGeehan, C. Williams, and A. Doufexi
Application of cooperative sensing in radar-communications coexistence
IET Commun., vol. 2, no. 6, pp. 856–868, Jul. 2008.
- [25] M. R. Bell, N. Devroye, D. Erricolo, T. Koduri, S. Rao, and D. Tuninetti
Results on spectrum sharing between a radar and a communications system
In *Proc. Int. Conf. Electromagn. Adv. Appl.*, Aug. 2014, pp. 826–829.
- [26] M. Bica, K.-W. Huang, U. Mitra, and V. Koivunen
Opportunistic radar waveform design in joint radar and cellular communication systems
In *Proc. IEEE Glob. Commun. Conf.*, Dec. 2015, pp. 1–7.
- [27] A. Lackpour, J. R. Guerci, A. Rosenwinkel, D. Ryan, and A. N. Mody
Design and analysis of an information exchange-based radar/communications spectrum sharing system (RCS3)
In *Proc. IEEE Radar Conf.*, May 2016, pp. 1–6.
- [28] C. D. Richmond, P. Basu, R. Learned, J. Vian, A. P. Worthen, and M. Lockard
Performance bounds on cooperative radar and communication systems operation
In *Proc. IEEE Radar Conf.*, May 2016, pp. 1–6.
- [29] M. P. Fitz, T. R. Halford, I. Hossain, and S. W. Enserink
Towards simultaneous radar and spectral sensing
In *Proc. IEEE Int. Symp. Dyn. Spectr. Access Netw.*, Apr. 2014, pp. 15–19.
- [30] A. D. Harper, J. T. Reed, J. L. Odom, and A. D. Lanterman
Performance of a joint radar-communication system in doubly-selective channels
In *Proc. 49th Asilomar Conf. Signals Syst. Comput.*, Nov. 2015, pp. 1369–1373.

- [31] S. Haykin
Cognitive radar: A way of the future
IEEE Signal Process. Mag., vol. 23, no. 1, pp. 30–40, Jan. 2006.
- [32] J. R. Guerci
Cognitive Radar: The Knowledge-Aided Fully Adaptive Approach (Artech House Radar Library). Norwood, MA, USA: Artech House, 2010.
- [33] P. Setlur and N. Devroye
Adaptive waveform scheduling in radar: An information theoretic approach
Proc. SPIE, vol. 8361, May 2012, Art. no. 836103.
- [34] Y. Nijsure, Y. Chen, C. Yuen, and Y. H. Chew
Location-aware spectrum and power allocation in joint cognitive communication-radar networks
In Proc. 6th Int. ICST Conf. Cogn. Radio Oriented Wireless Netw. Commun., Jun. 2011, pp. 171–175.
- [35] B. H. Kirk, R. M. Narayanan, K. A. Gallagher, A. F. Martone, and K. D. Sherbondy
Avoidance of time-varying radio frequency interference with software-defined cognitive radar
IEEE Trans. Aerosp. Electron. Syst., vol. 55, no. 3, pp. 1090–1107, Jun. 2019.
- [36] R. Palamã, H. Griffiths, and F. Watson
Joint dynamic spectrum access and target-matched illumination for cognitive radar
IET Radar, Sonar Navigat., vol. 13, pp. 750–759, May 2019.
- [37] B. Ravenscroft, J. W. Owen, J. Jakabosky, S. D. Blunt, A. F. Martone, and K. D. Sherbondy
Experimental demonstration and analysis of cognitive spectrum sensing and notching for radar
IET Radar, Sonar Navigat., vol. 12, pp. 1466–1475, Dec. 2018.
- [38] J. W. Owen, C. A. Mohr, B. H. Kirk, S. D. Blunt, A. F. Martone, and K. D. Sherbondy
Demonstration of real-time cognitive radar using spectrally-notched random fm waveforms
In Proc. IEEE Int. Radar Conf., 2020, pp. 123–128.
- [39] B. Ravenscroft *et al.*
Experimental assessment of joint range-doppler processing to address clutter modulation from dynamic radar spectrum sharing
In Proc. IEEE Int. Radar Conf., 2020, pp. 448–453.
- [40] A. Aubry, A. De Maio, M. Piezzo, M. M. Naghsh, M. Soltanalian, and P. Stoica
Cognitive radar waveform design for spectral coexistence in signal-dependent interference
In Proc. IEEE Radar Conf., May 2014, pp. 474–478.
- [41] Y. Nijsure, Y. Chen, S. Boussakta, C. Yuen, Y. H. Chew, and Z. Ding
Novel system architecture and waveform design for cognitive radar radio networks
IEEE Trans. Veh. Technol., vol. 61, no. 8, pp. 3630–3642, Oct. 2012.
- [42] K.-W. Huang, M. Bicã, U. Mitra, and V. Koivunen
Radar waveform design in spectrum sharing environment: Coexistence and cognition
In Proc. IEEE Radar Conf., May 2015, pp. 1698–1703.
- [43] A. F. Martone, K. A. Gallagher, and K. D. Sherbondy
Joint radar and communication system optimization for spectrum sharing
In Proc. IEEE Radar Conf., 2019, pp. 1–6.
- [44] S. Howard, W. Moran, A. Calderbank, H. Schmitt, and C. Savage
Channel parameters estimation for cognitive radar systems
In Proc. IEEE Int. Conf. Acoust., Speech, Signal Process., Mar. 2005, vol. 5, pp. 897–900.
- [45] S. Howard, A. Calderbank, and W. Moran
The finite Heisenberg-Weyl groups in radar and communications EURASIP J. Adv. Signal Process., vol. 2006, Apr. 2006, Art. no. 085685.
- [46] A. Pezeshki, A. R. Calderbank, W. Moran, and S. D. Howard
Doppler resilient Golay complementary waveforms
IEEE Trans. Inf. Theory, vol. 54, no. 9, pp. 4254–4266, Sep. 2008.
- [47] L. Xiaobai, Y. Ruijuan, Z. Zunquan, and C. Wei
Research of constructing method of complete complementary sequence in integrated radar and communication
In Proc. IEEE 11th Int. Conf. Signal Process., Oct. 2012, vol. 3, pp. 1729–1732.
- [48] M. Braun, C. Sturm, A. Niethammer, and F. K. Jondral
Parametrization of joint OFDM-based radar and communication systems for vehicular applications
In Proc. IEEE 20th Int. Symp. Pers. Indoor Mobile Radio Commun., Sep. 2009, pp. 3020–3024.
- [49] C. Sturm, T. Zwick, and W. Wiesbeck
An OFDM system concept for joint radar and communications operations
In Proc. IEEE 69th Veh. Technol. Conf., Apr. 2009, pp. 1–5.
- [50] Y. L. Sit, C. Sturm, L. Reichardt, T. Zwick, and W. Wiesbeck
The OFDM joint radar-communication system: An overview
In Proc. 3rd Int. Conf. Adv. Satell. Space Commun., Apr. 2011, pp. 69–74.
- [51] Y. L. Sit, L. Reichardt, C. Sturm, and T. Zwick
Extension of the OFDM joint radar-communication system for a multipath, multiuser scenario
In Proc. IEEE RadarCon, May 2011, pp. 718–723.
- [52] C. W. Rossler, E. Ertin, and R. L. Moses
A software defined radar system for joint communication and sensing
In Proc. IEEE Radar Conf., May 2011, pp. 1050–1055.
- [53] T. Guo and R. Qiu
OFDM waveform design compromising spectral nulling, sidelobe suppression and range resolution
In Proc. IEEE Radar Conf., May 2014, pp. 1424–1429.
- [54] S. C. Thompson and J. P. Stralka
Constant envelope OFDM for power-efficient radar and data communications
In Proc. Int. Waveform Diversity Des. Conf., Feb. 2009, pp. 291–295.
- [55] R. F. Tigrek, W. J. A. de Heij, and P. van Genderen
Relation between the peak to average power ratio and Doppler sidelobes of the multi-carrier radar signal
In Proc. Int. Radar Conf.—Surveillance Safer World, Oct. 2009, pp. 1–6.
- [56] C. E. Thornton, R. M. Buehrer, A. F. Martone, and K. D. Sherbondy
Experimental analysis of reinforcement learning techniques for spectrum sharing radar
In Proc. IEEE Int. Radar Conf., 2020, pp. 67–72.
- [57] T. M. Cover and J. A. Thomas
Elements of Information Theory, 2nd ed. Hoboken, NJ, USA: Wiley, 2006.
- [58] A. R. Chiriyath, B. Paul, G. M. Jacyna, and D. W. Bliss
Inner bounds on performance of radar and communications co-existence
IEEE Trans. Signal Process., vol. 64, no. 2, pp. 464–474, Jan. 2016.
- [59] B. Paul and D. W. Bliss
Extending joint radar-communications bounds for FMCW radar with Doppler estimation
In Proc. IEEE Radar Conf., May 2015, pp. 89–94.
- [60] B. Paul and D. W. Bliss
The constant information radar
Entropy, vol. 18, no. 9, 2016, Art. no. 338.
- [61] MATLAB's fmincon - Nonlinear Optimization - MathWorks © 2016. [Online]. Available: <https://www.mathworks.com/help/optim/ug/fmincon>



Shammi A. Doly received the B.Sc.(Eng.) degree in electrical and electronic engineering from the Ahsanullah University of Science and Technology, Dhaka, Bangladesh, in 2015, and the M.S. degree in electrical engineering from the South Dakota School of Mines and Technology, Rapid City, SD, USA, in 2021. She is currently working toward the Ph.D. degree with the BLISS Lab and the Center for Wireless Information Systems and Computational Architectures, Arizona State University, Tempe, AZ,

USA.

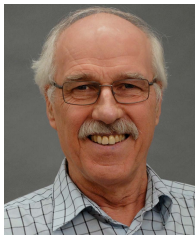
Before joining BLISS Lab, she was a Research Assistant with Unmanned and Swarm System Laboratory, South Dakota School of Mines and Technology, with Dr. Shankarachary Ragi. Her current research interests include distributed coherent systems and optimal control.



Alex R. Chiriyath received the B.S.E.E. degree (*cum laude*) from the University of Michigan at Ann Arbor, Ann Arbor, MI, USA, in 2012, and the M.S. and Ph.D. degrees from Arizona State University, Tempe, AZ, USA, in 2014 and 2018, respectively, all in electrical engineering.

In 2018, he joined as a Postdoctoral Researcher Arizona State University, where he has been an Assistant Research Professor with the BLISS Laboratory and the Center for Wireless Information Systems and Computational Architectures since 2021. His main research interests include radio frequency spectral convergence and flexible multifunction radio frequency systems.

USA.



Hans D. Mittelmann received the Habilitation degree and the Ph.D. degree in mathematics from the Technical University of Darmstadt, Darmstadt, Germany.

He is currently a Professor of Computational Mathematics with Arizona State University, Tempe, AZ, USA. Prior to his appointment, he was a Professor with the University of Dortmund, Dortmund, Germany. He has authored or coauthored 160 papers in computational mathematics, initially in the numerical solution of

partial differential equations, lately in interdisciplinary collaboration concentrating on optimization and applications. For more than 20 years, he has been maintaining two of the most frequented websites on optimization and related software. He evaluates a wide range of available programs for continuous and discrete optimization.



Daniel W. Bliss (Fellow, IEEE) received the B.S. degree in electrical engineering from Arizona State University (ASU), Tempe, AZ, USA, in 1989, and the Ph.D. degree in physics from the University of California at San Diego, San Diego, CA, USA, in 1997.

He is currently the Motorola Professor with the School of Electrical, Computer, and Energy Engineering, Arizona State University, where he is also the Director of Center for Wireless Information Systems and Computational Architectures.

Before joining ASU, he was a Senior Member of the Technical Staff with the MIT Lincoln Laboratory, Massachusetts Institute of Technology, Lexington, MA, USA, from 1997 to 2012. He has authored or coauthored two textbooks and more than 200 technical articles. He is responsible for foundational work in electronic protection, adaptive multiple-input multiple-output (MIMO) radar, MIMO communications, distributed-coherent systems, and radio frequency convergence. To enable implementation of these advanced systems, he has led coarse-scale heterogeneous system-on-chip development programs. He has served as a Principal Investigator on numerous projects, including sponsored programs with the Defense Advanced Research Projects Agency, the Office of Naval Research, Google, Airbus, and many others. Between his undergraduate and graduate degrees, he was with General Dynamics (from 1989 to 1993), where he designed avionics for the Atlas-Centaur launch vehicle and performed magnetic field optimization for high-energy particle-accelerator superconducting magnets. His doctoral work (1993–1997) was in the area of high-energy particle physics and lattice gauge theory calculations.

Dr. Bliss is the recipient of the 2021 IEEE Warren D. White Award for Excellence in Radar Engineering. He is a member of the Editorial Board of *IEEE Signal Processing Magazine*.



Shankarachary Ragi (Senior Member, IEEE) received the B.Tech. and M.Tech. degrees in electrical engineering from the Indian Institute of Technology Madras, Chennai, India, in 2009, and the Ph.D. degree in electrical and computer engineering from Colorado State University, Fort Collins, CO, USA, in 2014.

He is currently an Assistant Professor with the Department of Electrical Engineering, South Dakota School of Mines and Technology, Rapid City, SD, USA. Before joining the South Dakota School of Mines and Technology, he was a Postdoctoral Researcher with the Department of Mathematics, Arizona State University, Tempe, AZ, USA. Prior to that, he was a Senior Control Engineer with Cummins Emission Solutions. He has authored or coauthored more than 29 peer-reviewed publications in various journals and conference proceedings. His current research interests include machine learning, image analysis, robotics, and optimal control.

Dr. Ragi was an Associate Editor for IEEE ACCESS from 2017 to 2020.